

Development of a Spherical Ultrasonic Motor with an Attitude Sensing System using Optical Fibers

Tomoaki Mashimo, Kosuke Awaga, and Shigeki Toyama

*Department of Mechanical Systems Engineering
Tokyo University of Agriculture and Technology
2-24-16 Nakacho, Koganei, Tokyo, 184-8588, Japan*

E-mail: t-masimo@cc.tuat.ac.jp, Phone: +81-42-388-7098, Fax: +81-42-388-7207

Abstract— We present a spherical ultrasonic motor (SUSM) and an attitude sensing system using optical fibers for the SUSM. The SUSM is constructed from three ring-shaped stators and a spherical rotor, and has three degrees of freedom (DOF). It has good responsiveness, high positioning accuracy, and strong magnetic field compatibility. In the attitude sensing system, a flat mirror is built in the spherical rotor. Light is emitted to the mirror, and the reflection is caught by optical fibers. The light intensities captured by the optical fibers are processed by a neural network and are converted to attitude information for the spherical rotor. We describe a system comprising the SUSM and the attitude sensing system with its design derived from mechanics and optics. The prototype SUSM is 26mm in diameter and was actuated by the attitude sensing system. Position errors with respect to x and y axes are less than 0.5°.

Index Terms— Spherical ultrasonic motor, attitude sensing, geometrical optics, neural network.

I. INTRODUCTION

Spherical motors with a single spherical rotor have potential application in the next generation of robots, including ubiquitous robots and surgical robots. They have more than one degree of freedom (DOF) in a single joint, like the eyes, wrist, and shoulder. In a future ubiquitous society, spherical motors can drive the motion of robots. A number of reports exist of spherical motors. Most work has focused on driving sources based on an electromagnetic motor, such as a stepping motor [1]-[5], an induction motor [6] or a direct current motor.

We have also developed a spherical motor, which we call a spherical ultrasonic motor (SUSM). Our previous study was the first attempt to apply the ultrasonic motor as a spherical motor [7]. Compared with spherical motors that use electromagnetic power, it has high responsiveness because of the friction drive principle, and high positioning accuracy because of the piezoelectric effect. Piezoelectric actuators are occasionally used for precise positioning in industrial applications. Ultrasonic motors have the characteristic of high torque at low speed without a reduction gear. Their simple structure allows for efficient miniaturization. Because electromagnetic power is not used for its actuation, it may be rotated in the presence of strong magnetic fields. Ultrasonic motors are used in devices requiring strong magnetic field,

such as magnetic resonance imaging (MRI) scanners and a linear motor in an experimental stage.

In Ref. [7], the SUSM used four stators. Its drive was unstable, however, because of its structure in which crosswise opposite stators hold a spherical rotor. Each preload of two sets of the opposite stators is unequal. A SUSM having four stators seldom gives a repeatable performance. In Ref. [8], a fine orientating stage using three stators was developed. This showed superior accuracy.

Other spherical motors using the ultrasonic motor principle also have the characteristics noted above. Ueha et al., Maeno et al., and Aoyagi et al. have proposed a differently shaped spherical motor using the ultrasonic motor principle. Their spherical motor with three DOF is composed of a spherical rotor and a bar-shaped stator [9]-[11]. Ueha's spherical motor has been applied to a head robot that has a three-DOF neck mechanism, as an auditory tele-existence robot [12]. In ref. [13] the concept is applied to a master-slave laparoscopic forceps manipulator, exploiting the compactness, dexterity and multiple DOF of the motor for minimally invasive surgery.

Consider now the attitude sensing method of spherical motors. The term "attitude" is defined as the orientation of the spherical rotor. A few studies have been made of the attitude sensing system that exploits the advantages of the spherical motors. In previous attitude sensing methods, spherical motors have been used in rotary encoders [7], [14], potentiometers [13], hole sensors [3], [15], and a two-dimensional position sensitive detector (PSD) [16]. In Ref. [14], three rotary encoders measure the three DOF rotation with the guide mechanism for the spherical motor. Maeno uses potentiometers to measure the two DOF rotation of a spherical motor using a bar-shaped ultrasonic motor [13]. A key advantage of a spherical motor that employs an ultrasonic motor is compactness. However, rotary encoders and potentiometers are needed to guide the rotation, and the sensing devices cause the spherical motor to be large. These sensing methods lose the advantage of compactness. On the other hand, although PSD has good responsiveness, it is expensive. Wang et al. uses four hole sensors for a 2 DOF spherical synchronous motor [3]. Stein et al. developed an

optical encoder for spherical motion. The spherical rotor is painted black and white; many optical sensors detect these colors [17].

Using a standard approach, we aimed to develop a rotary encoder and hole sensor [7], [15]. In the rotary encoder, the spherical motor attached to the rotary encoders has good attitude sensing. Unfortunately it is large, losing the advantages of miniaturization of the SUSM. Many components are also needed for the guide parts. In the case of the hole sensor, the spherical motor attached to the hole sensors is very compact. However, the positioning accuracy is poor, and the SUSM cannot be used in a strong magnetic field environment. Sensing using hole sensors also loses the advantages of the SUSM.

In one sensing method, optical sensors measure the spherical rotor painted in black and white, but it is difficult to paint our spherical rotor because of its small size; also, there is no space for installation of many sensors. An image sensor and image processing device is often used for position sensing in manufacturing processes. Application to sensing for spherical motors has been developed [18]. The use of image sensors loses the advantages of high responsiveness. Consequently, we have developed a new attitude sensing system for optimal drive of the SUSM.

In the present study, a novel SUSM has been constructed, composed of non-magnetic materials with a new attitude sensing system that uses optical fibers and a spherical rotor attached to a flat mirror. The motion mechanism of the SUSM and the optical principle of the attitude sensing are described. Accurate driving of the SUSM using the attitude sensing system proves successful.

II. MECHANISM OF THE SUSM

The SUSM is composed of three stators and a spherical rotor, and produces an angular velocity vector with three DOF by the arrangement of the stators. The coordinates are defined in Fig.1. The three stators are placed such that the angle between them is 120° , and they are make an (arbitrary) angle α° with the x-y plane. The composition vector resulting from the angular velocity vector of each stator has a nonzero component along each axis. Consequently, the rotor can move with three DOF. Taking the origin at the center of the rotor, and the z-axis as the vertical, the plane that intersects the origin perpendicular to the z-axis is the x-y plane. We take the x-axis to be the line from the origin passing through the stator S1, and the y-axis as the line passing through the origin perpendicular to the x-axis and z-axis. The target angular velocity vector $\boldsymbol{\omega}$ is obtained by combining the angular velocity vectors $\boldsymbol{\omega}_1$, $\boldsymbol{\omega}_2$, and $\boldsymbol{\omega}_3$ resulting from these stators, which can be expressed as

$$\boldsymbol{\omega} = \boldsymbol{\omega}_1 + \boldsymbol{\omega}_2 + \boldsymbol{\omega}_3 \quad (1)$$

$$\boldsymbol{\omega} = \omega_1 \mathbf{u}_1 + \omega_2 \mathbf{u}_2 + \omega_3 \mathbf{u}_3 \quad (2)$$

where ω_1 , ω_2 , and ω_3 , are scalar magnitudes of the angular

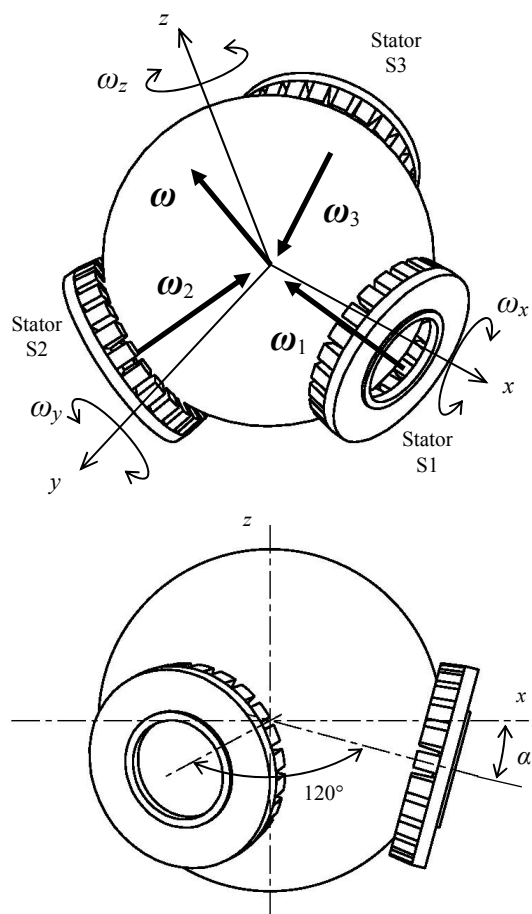


Fig.1 Mechanism of the SUSM

velocity vectors generated by stators S1, S2 and S3. They depend on the applied magnitude, frequency and phase difference of the voltage applied to the stators. Here \mathbf{u}_1 , \mathbf{u}_2 , and \mathbf{u}_3 are unit vectors in the direction of the angular velocity vector that each stator generates, and are expressed as

$$\mathbf{u}_1 = [-\cos \alpha \quad 0 \quad \sin \alpha]^T \quad (3)$$

$$\mathbf{u}_2 = \left[\frac{1}{2} \cos \alpha \quad -\frac{\sqrt{3}}{2} \cos \alpha \quad \sin \alpha \right]^T \quad (4)$$

$$\mathbf{u}_3 = \left[\frac{1}{2} \cos \alpha \quad \frac{\sqrt{3}}{2} \cos \alpha \quad \sin \alpha \right]^T \quad (5)$$

From Eqs (3)-(5), the target angular velocity vector $\boldsymbol{\omega}$ is calculated as

$$\boldsymbol{\omega} = [\omega_x \quad \omega_y \quad \omega_z]^T$$

$$\boldsymbol{\omega} = \begin{bmatrix} \left(-\omega_1 + \frac{1}{2}\omega_2 + \frac{1}{2}\omega_3\right) \cos \alpha \\ \left(-\frac{\sqrt{3}}{2}\omega_2 + \frac{\sqrt{3}}{2}\omega_3\right) \cos \alpha \\ (\omega_1 + \omega_2 + \omega_3) \sin \alpha \end{bmatrix} \quad (6)$$

From these expressions, it follows that the angular velocity vector $\boldsymbol{\omega}$ is determined by the arrangement of the stators and the angular velocity that each stator sets up.

III. PRINCIPLE OF THE ATTITUDE SENSING

A new attitude sensing method was developed for the SUSM. Fig.2 shows a schematic of this sensing method. The flat mirror is attached to the spherical rotor. Light from a laser diode passes through an optical fiber and is emitted to the mirror. The reflection is caught by the tip of some optical fibers and is carried to a photodiode. When the spherical rotor turns, the direction of the reflection changes. The light intensity carried to the photodiode also changes, and the light intensity is converted to positional information by a computer. This is similar to the principle of optical switches. The method has the following advantages. (i) The attitude sensing system works in strong magnetic environments because it does not use electric parts in the environment; (ii) It has high accuracy, because the position is decided by continuously optical intensities; (iii) It can be small, because the only tips of the optical fibers are installed the SUSM; (iv) All parts of the system are cheap (e.g. laser diode, photodiode, and plastic optical fibers).

The principle of the attitude sensing using a spherical rotor attached to a flat mirror and optical fibers is described geometrically by a two-dimensional model, as shown in Fig.3. Let the spherical rotor rotate around the z-axis. If the rotational angle of the spherical rotor is θ , then the center point $Q(r, 0)$ moves to $Q'(r \cos \theta, r \sin \theta)$. The reflectional point $P(x_p, y_p)$ is specified by the positional relation between the tip of an emitting optical fiber and that of a detecting optical fiber. Since the points Q' and P are on the line vector \boldsymbol{M} drawn from the surface of the flat mirror, the relation between the point $P(x_p, y_p)$ and the rotational angle of the spherical rotor θ is given by

$$y_p + \frac{x_p}{\tan \theta} = r \sin \theta + \frac{r \cos \theta}{\tan \theta} \quad (7)$$

where r is the distance between the center point of the spherical rotor and the center point of the flat mirror. The line vector \boldsymbol{R}_e connects the point P and the tip of the emissive optical fiber. The line vector \boldsymbol{R}_d connects the point P and the tip of the detective optical fiber. The normal to the surface of the flat mirror is expressed by the line vector \boldsymbol{N} and passes

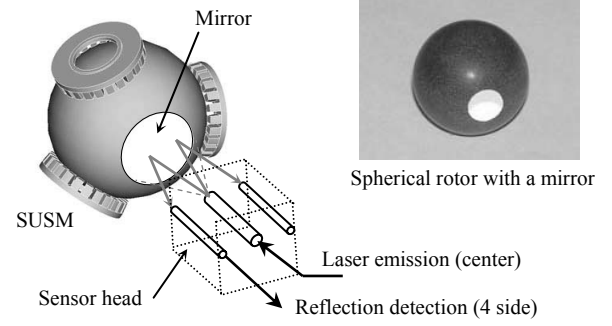


Fig.2 Schematic of the attitude sensing of the SUSM

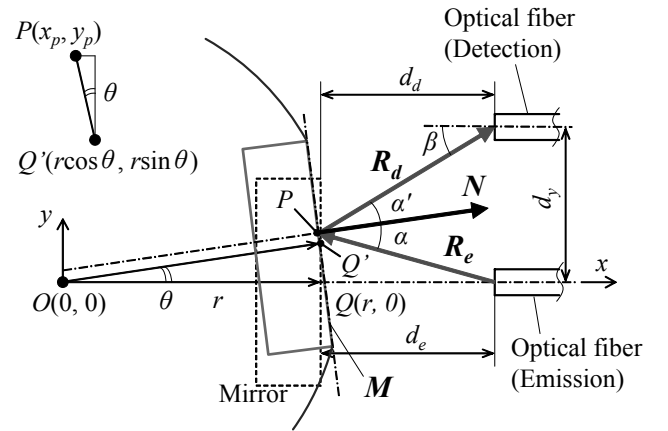


Fig.3 Optical model of the sensing (x-y plane model)

through the point P . The incidence angle α is equal to α' ,

$$\tan^{-1} \nabla \boldsymbol{R}_e + \tan^{-1} \nabla \boldsymbol{N} = \tan^{-1} \nabla \boldsymbol{R}_d - \tan^{-1} \nabla \boldsymbol{N} \quad (8)$$

where

$$\nabla \boldsymbol{R}_e = y_p / (r + d_e - x_p) \quad (9)$$

$$\nabla \boldsymbol{R}_d = (d_y - y_p) / (r + d_d - x_p) \quad (10)$$

where and $\nabla \boldsymbol{N}$ is $\tan \theta$, d_e is the distance between the tip of the emissive optical fiber and surface of the mirror at $\theta=0$, and d_d are the distance to the tip of the detective fiber from the surface of the mirror. d_y is the distance between the emissive optical fiber and detective optical fiber in the y-direction. From Eqs. (8)-(10):

$$\tan^{-1} \left(\frac{d_y - y_p}{r + d_d - x_p} \right) - \tan^{-1} \left(\frac{y_p}{r + d_e - x_p} \right) = 2\theta \quad (11)$$

From Eqs. (7) and (11), the point $P(x_p, y_p)$ is specified on the surface of the mirror when the angle θ is given. Here, the point P cannot be placed over the radius of the spherical rotor r_r :

$$\sqrt{x_p^2 + y_p^2} \leq r_r \quad (12)$$

The surface of the flat mirror is protected from scratches by stators when the spherical rotor turns. The surface of the flat mirror should be lower than that of the spherical rotor, and the inner radius of the stators is larger than the diameter of the flat mirror.

The light intensity I from the tip of the emissive optical fiber to the flat mirror conforms to the Gaussian distribution:

$$I = I_0 \exp(-2\rho^2 / w_z^2) \quad (13)$$

where I_0 is the light intensity at the light axis, ρ is the distance from the light axis when $\theta=0$, and w_z is the beam radius obtained experimentally. Supposing that the light intensities at the point P and the distance ρ are equal to each other, the equation of the line vector R_e is given by

$$y = \frac{y_p}{r + d_e - x_p} (r + d_e - x) \quad (14)$$

Based on the light intensity distribution at the mirror surface in the case of $\theta=0$ then x equals r , and the distance from the light axis ρ is given by

$$\rho = \frac{y_p}{r + d_e - x_p} d_e \quad (15)$$

On the other hand, the detection rate changes with the position of the detecting optical fiber and the direction of reflection. The detection rate A also follows a Gaussian distribution and is given by

$$A = \exp(-2\beta^2 / w_A^2) \quad (16)$$

where β is the detection angle and $\beta=\alpha'+\theta$. Here w_A is the beam radius, obtained experimentally. Thus, when the rotational angle θ is given, the light intensity I_r caught by the detecting optical fiber catches is

$$I_r = A I_0 \exp(-2\rho^2 / w_z^2) \quad (17)$$

However, it is difficult to obtain high positioning accuracy of the SUSM. The reasons include differences in the surface of the optical fiber tips, reflections where the optical fibers are held and at the interface between optical fibers and photo diodes. A neural network, acting as a multi input multi output nonlinear system, is used as a converter to the positional information.

IV. PROTOTYPE AND EXPERIMENT

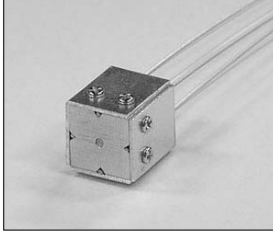
A. Prototype of the SUSM with the attitude sensing system

A SUSM embedded optical fibers was developed as a prototype. The designs of the SUSM and the sensor head of the sensing system are shown in Figs.5 and 6; fig.7 shows a schematic of the driving and sensing system. The attitude sensing system is constructed of a laser diode circuit, sensor head, the mirror attached to the spherical rotor, a photodiode



Rotor material	Bakelite
Rotor diameter	φ20mm
Stator material	Phosphor bronze
Stator size	φ12mm
Preload (Calculated value)	5N
Entire size	26mm
Mirror diameter	φ6.35mm
Radius r	9.3mm
Inclination α	0°

Fig.5 Newly assembled SUSM



d_e	5.5mm
d_d	5.5mm
d_y	4.75mm
d_z	4.75mm
Diameter of emission fiber (Center)	φ1.0mm
Diameter of detection fibers (Four side)	φ0.5mm

Fig.6 Sensor head of the position sensing system

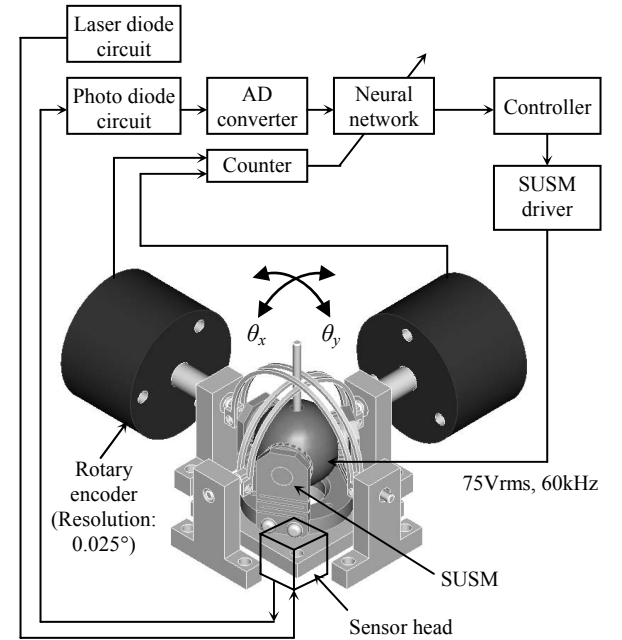


Fig.7 Schematic of the driving and sensing system of SUSM

circuit, and a computer including the neural network algorithm. Two rotary encoders, having resolution 0.025°, are used in learning data for the neural network and in measuring the absolute coordinate in trajectory control experiments. The applied voltage the SUSM driver generates is approximately 75 V_{rms}, and the applied frequency is about 60 kHz. The angle of the experimental device defined from the vertical direction (z-axis in Fig.1) is 0°. The rotational angles θ_x and θ_y are provided by the output of the two rotary encoders.

The accuracy of the SUSM without the attitude sensing

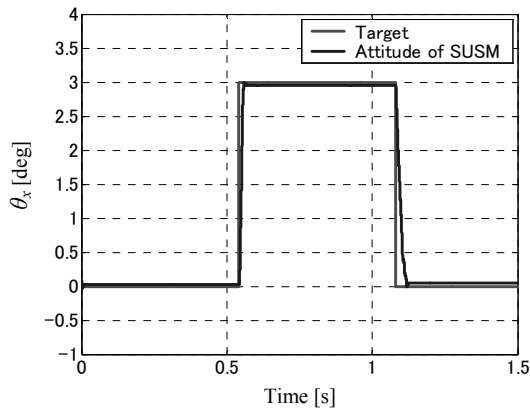


Fig.8 Positioning accuracy of the SUSM

system is first measured in a step response test. The input is from 0° to $+3^\circ$ as target position. The experimental results are shown in Fig.8. The SUSM have demonstrated high positioning accuracy less than 0.05° . This accuracy is limited by the resolution of the rotary encoder; in Ref. [8], the SUSM has indicated better accuracy.

B. Verification of the optical simulation

The light intensity was calculated based on the eqs. (7)-(17). It was compared with an experimental result using the measurement device of Fig.7 Here, the rotation of θ_y is fixed and the spherical rotor rotates only the direction of θ_x . The result is shown in Fig.9. The light intensity has been converted to a voltage by the photodiode circuit. The predictions are in broad agreement with the experimental data. The experimental result is little higher than the simulational result at the frequency range of -1 kHz to 9kHz. The reason is that the first reflection from the mirror reflects again off the sensor head. Accordingly, the rereflection has heightened the light intensity.

C. Position data converter using a neural network

The reflection intensity from four optical fibers is converted to voltage in the photodiode circuit. The distributions of the light intensity of each optical fiber are measured over a range of $\pm 5^\circ$ with respect to the x- and y-axes in Fig.1. The respective distributions are shown in Fig.10. A neural network converts the light intensity data to attitude data. The light intensities from four optical fibers and two attitude data θ_x and θ_y from two rotary encoders are used for the supervised learning by the neural network. The neural network consists of an input layer, a hidden layer, and an output layer as shown in Fig.11. Forty sigmoids are used in the hidden layer. Supervised learning is conducted at 0.5° intervals using the attitude data θ_x and θ_y of two rotary encoders as learning data in the $\pm 5^\circ$ sensing range. 21 points in each of the x- and y-directions, and therefore $21 \times 21 = 441$ datapoints in total, are captured for the supervised learning.

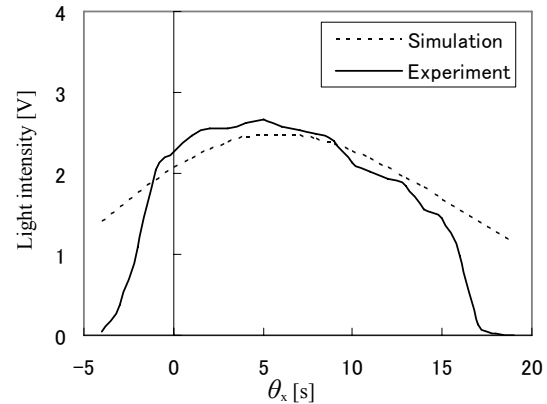


Fig.9 Positioning accuracy of the SUSM

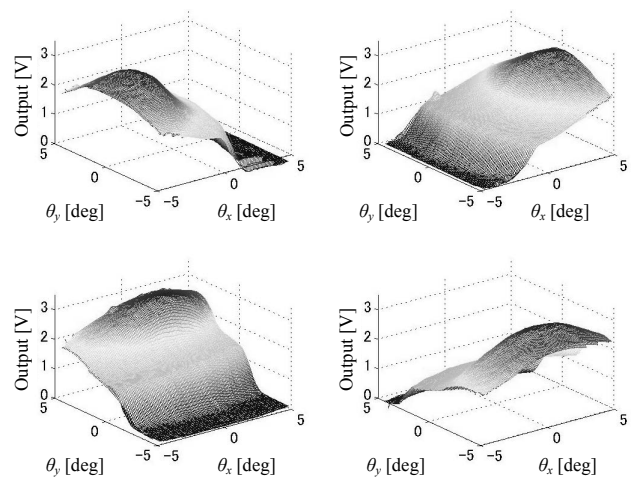


Fig.10 Distribution of the reflection intensity of each optical fiber

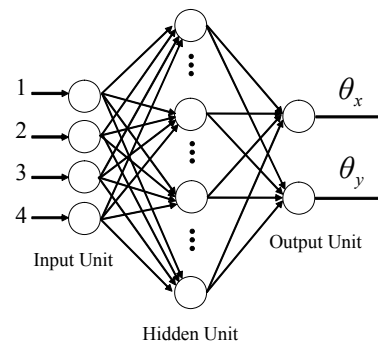


Fig.11 Model of neural network

D. Trajectory control using optical sensing system

The target paths make up a quadrate and a circle drawn by $\pm 5^\circ$ (approximately 1.75mm on the surface of the spherical rotor). When the SUSM was controlled, 74 points were sampled on the quadratic path and 63 points were sampled on

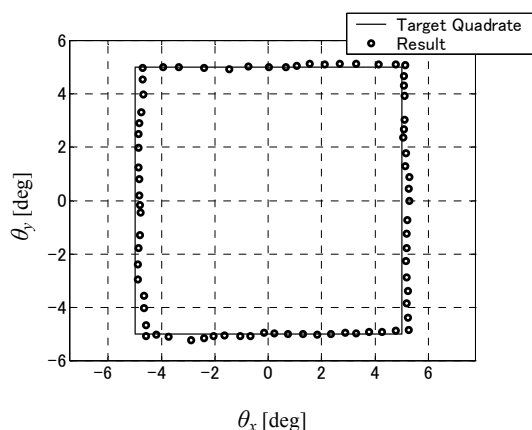


Fig.12 Trajectory control (Quadrate)

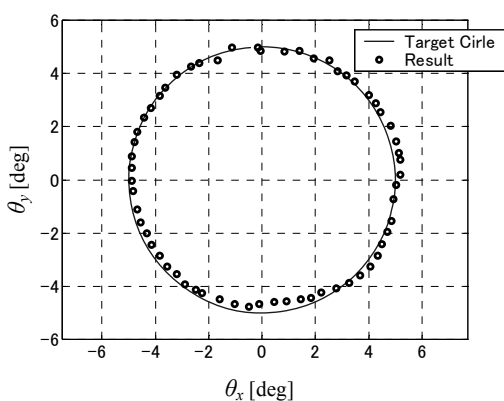


Fig.13 Trajectory control (Circle)

the circular path. These experimental results are shown in Figs.12 and 13, which show that the SUSM has good controllability and that the attitude sensing system is effective for control. The maximum error of the position is less than 0.5° , which corresponds to less than $87\ \mu\text{m}$ on the surface of the spherical rotor. The error is a limiting value, because it is similar to the 0.5° interval used in the supervised learning. Most of the trajectory errors cause the noises from the photodiode circuit. The photocurrent-to-voltage converter and amplifier circuit include electronic noises.

V. CONCLUSION

We have demonstrated a novel SUSM, of diameter 26 mm, with an attitude sensing system that uses optical fibers. The attitude sensing system allows the resulting device to fully exploit the advantages of the SUSM. Compared against other sensing methods for spherical motors, it achieves high accuracy, compactness, low cost, and robustness in strong magnetic fields. In future, the mirror of the spherical rotor will be changed to large mirror and/or an unlevel surface mirror to increase the sensing range and accuracy. In the experiment, a single sensor head was used with four detective optical fibers. If the learning data are increased in number, the attitude sensing system can attain greater accuracy. Increasing the number of sensor heads and optical fibers is

also effective. Although we successfully obtained high accuracy using the neural network, the supervised learning process needs a certain learning time. As long as the same optical conditions are fulfilled, the sensing system can find the attitude quickly and accurately without additional training time. Ideally, an attitude sensing system without the neural network process should be developed based on the optical theory.

REFERENCES

- [1] K. M. Lee, R. Roth, and Z. Zhou, "Dynamic modeling and control of a ball-joint-like VR spherical motor," *Trans. ASME Journal of Dynamic Systems, Measurement, and Control*, vol. 118, pp. 29-40, 1996.
- [2] G. S. Chirikjian and D. Stein, "Kinematic design and commutation of a spherical stepper motor," *IEEE/ASME Trans. Mechatronics*, vol. 4, pp. 342-353, Dec. 1999.
- [3] J. Wang, K. Mitchell, G. W. Jewell, and D. Howe, "Multi-degree-of-freedom spherical permanent magnet motors," in *Proc. IEEE International Conference on Robotics and Automation*, 2001, pp. 1798-1805 vol.2.
- [4] K. Kahlen, I. Voss, C. Priebe, and R. W. D. Doncker, "Torque control of a spherical machine with variable pole pitch," *IEEE Trans. Power Electronics*, vol. 19, pp. 1628-1634, Nov. 2004.
- [5] Q. Wang, Z. Li, Y. Ni, and W. Jiang, "Magnetic Field Computation of a PM Spherical Stepper Motor Using Integral Equation Method," *IEEE Trans. Magnetics*, vol. 42, pp. 731-734, April 2006.
- [6] B. Dehez, G. Galary, D. Grenier, and B. Raucent, "Development of a Spherical Induction Motor With Two Degrees of Freedom," *IEEE Trans. Magnetics*, vol. Accepted for publication, pp. 1-13, 2006.
- [7] S. Toyama, S. Sugitani, G. Zhang, Y. Miyatani, and K. Nakamura, "Multi degree of freedom spherical ultrasonic motor," in *Proc. IEEE International Conference on Robotics and Automation*, 1995, pp. 2935-2940.
- [8] E. Purwanto and S. Toyama, "Development of an ultrasonic motor as a fine-orienting stage," *IEEE Trans. Robotics and Automation*, vol. 17, pp. 464-471, Aug. 2001.
- [9] T. Amano, T. Ishii, K. Nakamura, and S. Ueha, "An ultrasonic actuator with multidegree of freedom using bending and longitudinal vibrations of a single stator," in *Proc. IEEE International Ultrasonics Symposium*, 1998, pp. 667-670.
- [10] K. Takemura and T. Maeno, "Design and control of an ultrasonic motor capable of generating multi-DOF motion," *IEEE/ASME Trans. Mechatronics*, vol. 6, pp. 499-506, Dec. 2001.
- [11] M. Aoyagi, S. P. Beeby, and N. M. White, "A novel multi-degree-of-freedom thick-film ultrasonic motor," *IEEE Trans. Ultrasonics, Ferroelectrics and Frequency Control*, vol. 49, pp. 151-158, Feb. 2002.
- [12] H. Kawano, H. Ando, T. Hirahara, C. Yun, and S. Ueha, "Application of a multi-DOF ultrasonic servomotor in an auditory tele-existence robot," *IEEE Trans. Robotics*, vol. 21, pp. 790-800, 2005.
- [13] S. Park, K. Takemura, and T. Maeno, "Study on multi-DOF ultrasonic actuator for laparoscopic instrument," *Bulletin of JSME, Series C*, vol. 47, pp. 574-581, June 2004.
- [14] K. M. Lee and C. K. Kwan, "Design concept development of a spherical stepper for robotic applications," *IEEE Trans. Robotics and Automation*, vol. 7, pp. 175-181, 1991.
- [15] E. Purwanto and S. Toyama, "Control method of a spherical ultrasonic motor," in *Proc. IEEE/ASME International Conference on Advanced Intelligent Mechatronics*, 2003, pp. 1321-1326.
- [16] K. IOI, K. SASAE, Y. Ohtsuki, and Y. Kurosaki, "Development of a miniature 3 DOF rotational actuator," in *International Symposium on Microsystems, Intelligent Materials and Robots*, 1995.
- [17] D. Stein, E. R. Scheinerman, and G. S. Chirikjian, "Mathematical models of binary spherical-motion encoders," *Mechatronics, IEEE/ASME Transactions on*, vol. 8, pp. 234-244, 2003.
- [18] K. M. Lee and Z. Debao, "A real-time optical sensor for simultaneous measurement of three-DOF motions," *Mechatronics, IEEE/ASME Transactions on*, vol. 9, pp. 499-507, 2004.